

Generation of a two-photon state from a quantum dot in a microcavity

E del Valle^{1,4}, A Gonzalez–Tudela², E Cancellieri², F P Laussy³ and C Tejedor²

¹ Physikdepartment, Technische Universität München, James-Frank-Strasse 1, 85748 Garching, Germany

² Física Teórica de la Materia Condensada, Universidad Autónoma de Madrid, 28049 Madrid, Spain

³ Walter Schottky Institut, Technische Universität München, Am Coulombwall 3, 85748 Garching, Germany

E-mail: elena.delvalle.reboul@gmail.com

New Journal of Physics **13** (2011) 113014 (12pp)

Received 8 July 2011

Published 11 November 2011

Online at <http://www.njp.org/>

doi:10.1088/1367-2630/13/11/113014

Abstract. We propose and characterize a two-photon (2P) source that emits in a highly polarized, monochromatic and directional beam, realized by means of a quantum dot embedded in a linearly polarized cavity. In our scheme, the cavity frequency is tuned to half the frequency of the biexciton (two excitons with opposite spins) and largely detuned from the excitons thanks to the large biexciton binding energy. We show how the emission can be Purcell enhanced by several orders of magnitude into the 2P channel for available experimental systems.

⁴ Author to whom any correspondence should be addressed.

Contents

1. Introduction	2
2. Mechanism of two-photon (2P) emission	3
3. Demonstration of the 2P emission at the 2P resonance	6
4. Efficiency of the 2P emission	9
5. Conclusions and outlook	10
Acknowledgments	10
References	11

1. Introduction

Two photons can be used as fundamental building blocks for an extended range of Quantum Information Processing protocols, with applications in quantum metrology [1], quantum communication and cryptography [2–4], linear-optics quantum computation [5–9] and even for fundamental tests of quantum mechanics such as hidden variable interpretations [10, 11]. A number of devices have been proposed and experimentally demonstrated with atomic gases [12–14] or nonlinear crystals [1, 15, 16]. The realization of such devices, however, is a highly nontrivial task since, in order to be useful, the generated photons need to be almost identical, narrow-band and generated with a high repetition rate. Useful quantum states made from two photons include pairs of identical photons, which are, however, not necessarily superimposed in space and/or in time, and the two-photon (2P) Fock states $|2\rangle$ where the two photons share the same attributes in their energy, space and time profile, encoding the information in their polarization. Standard protocols for quantum computation may rely on non-superimposed photon pairs [2], but 2P states can be used for more efficient quantum computation [7].

Some of us and coworkers have recently proposed a 2P generation scheme based on a single quantum dot embedded in a microcavity [17], which theoretically fulfils all the above requirements and, moreover, as it is based on semiconductors, is particularly promising for optical access, on-chip integration, output-collection and scalable technological implementations [18–21]. The principle relies on the biexciton (the occupation of the quantum dot by two excitons of opposite spins) being brought in resonance with twice the cavity photon energy. Thanks to the large biexciton binding energy, single-photon processes are detuned and are thus effectively suppressed, while simultaneous 2P emission is Purcell enhanced [17]. This effect has been recently demonstrated experimentally [22]. In the experiment, as in the initial proposal, the signature for the 2P emission is a strong emission enhancement of the cavity mode when hitting the biexciton 2P resonance. Because of incoherent excitation used in both the theoretical proposal and its experimental realization, the quantum character of the 2P emission is not directly demonstrated or quantified.⁵ Here, we upgrade to a configuration that is nowadays experimentally accessible, where the quantum dot is initially prepared in a pure biexciton state, and we analyze in detail the underlying microscopic mechanisms, demonstrating the perfect 2P character of the emission beyond a mere enhancement at the expected energy. We show how the 2P state is created by the system in a chain of virtual processes that cannot be broken

⁵ The authors of [22] also realize this limitation and speculate on the scheme that we analyze here in detail.

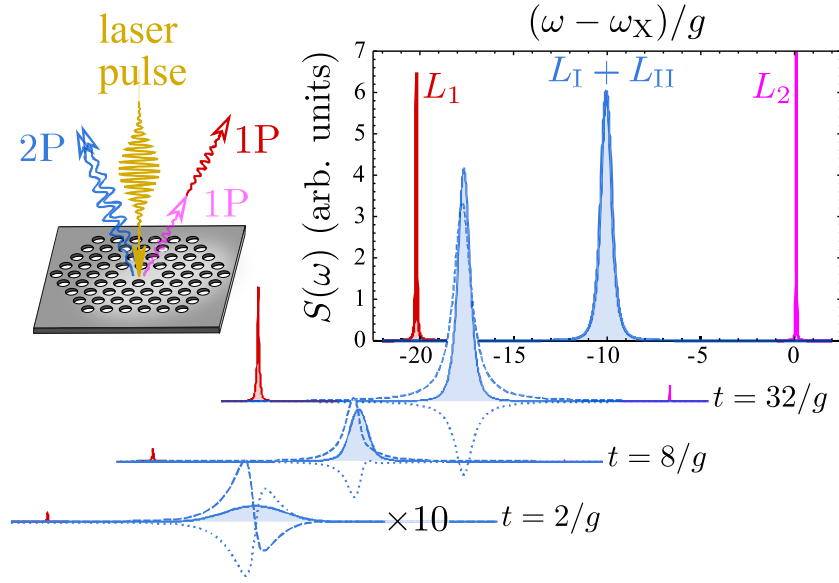


Figure 1. Cavity spectra of emission $S(t, \omega)$ at the 2P resonance for different times (unframed) and integrated over all times (framed). They feature the 2P peak at $\omega_a \approx -\chi/2$ (central, blue), with total intensity $L_I + L_{II}$, and the two 1P peaks at $\omega_1 \approx -\chi$ (left, red) and $\omega_2 \approx 0$ (right, pink), with intensities L_1 and L_2 . The physical processes giving rise to these peaks are spelled out in figure 2(b) with the same color code. The 2P peak cannot be decomposed into two separate physical processes. Parameters: $\chi = 20g$, $\kappa = g$ and $\gamma = 5 \times 10^{-4}g$.

apart in physical one-photon states. Our understanding is analytical and allows for optimization of a practical setup, enabling the realization of an efficient source of two simultaneous and indistinguishable photons in a monolithic semiconductor device.

2. Mechanism of two-photon (2P) emission

The characteristic spectral profile of the cavity-assisted 2P emission is shown in figure 1, with a central peak that is strongly enhanced at the 2P resonance, corroborating its 2P character, and surrounded by standard (single-photon) de-excitation [17, 22]. The 2P peak is spectrally narrow and isolated from the other events, which can never be completely avoided, so the source is appealing on practical grounds. The Hamiltonian of the system reads [17]

$$H(t) = (\omega_a - \omega_L)a^\dagger a + \sum_{i=\uparrow, \downarrow} (\omega_X - \omega_L)\sigma_i^\dagger \sigma_i - \chi \sigma_\uparrow^\dagger \sigma_\uparrow \sigma_\downarrow^\dagger \sigma_\downarrow + \sum_{i=\uparrow, \downarrow} \left[g_i (a^\dagger \sigma_i + a \sigma_i^\dagger) + \Omega_i(t)(\sigma_i + \sigma_i^\dagger) \right], \quad (1)$$

where we have included $i = \uparrow, \downarrow$ the spin-up and spin-down degrees of freedom for the excitonic states σ_i (fermions) with common frequency ω_X and a the cavity field annihilation operator (boson) with frequency ω_a . The cavity mode should have a strong polarization, say linearly polarized in the horizontal direction for a photonic crystal, a case we shall assume in the following. The biexciton binding energy χ allows us to bring the biexciton energy ω_B in

resonance with the 2P energy while detuning all other excitonic emissions from the cavity mode. It is red (blue) shifted if the biexciton is ‘bound’ (‘antibound’), giving rise to a positive $\chi > 0$ (negative $\chi < 0$) binding energy $\chi = 2\omega_X - \omega_B$. Our scheme works with both the bound and the antibound biexciton. Without loss of generality, we assume $\chi > 0$, with the added advantage of being less affected by pure dephasing and coupling to phonons [23], which we neglect. This binding energy is typically large ($\chi \approx 400\text{--}3000 \mu\text{eV}$) as compared to all the parameters in the system [22, 24], which is ideal for our purpose. It is for instance much larger than the fine structure splitting between excitonic states ($\approx 10 \mu\text{eV}$), even though in our case, this splitting is not detrimental to the mechanism as will be shown later.

We will assume an equal coupling of both excitons to the linearly polarized mode of the cavity, $g_\uparrow = g_\downarrow = g/\sqrt{2}$, and take g as the unit in the remainder of the text.⁶ The Hilbert space of the quantum dot is spanned, in its natural basis of circular polarization, by the ground $|G\rangle$, spin-up $|\uparrow\rangle$, spin-down $|\downarrow\rangle$ and biexciton $|B\rangle$ states. In the linearly polarized basis, the excitonic states are $|H\rangle = (|\uparrow\rangle + |\downarrow\rangle)/\sqrt{2}$ and $|V\rangle = (|\uparrow\rangle - |\downarrow\rangle)/\sqrt{2}$. The dot–cavity joint Hilbert space includes the photonic number n : $|j, n\rangle$, where $j = G, V, H$ and B , with $n \in \mathbb{N}$.

The quantum dot is excited by a laser of amplitude $\Omega_i(t)$ and frequency ω_L , which brings it in the biexciton state through 2P absorption. This can be realized via two appropriate coloured pulses [25, 26] or, more efficiently, by a single pulse spectrally matching the direct 2P absorption [24], $\omega_L = \omega_B/2 = \omega_X - \chi/2$. The laser polarization should be taken orthogonal to that of the cavity, $\Omega_\uparrow(t) = -\Omega_\downarrow(t) = \Omega(t)/\sqrt{2}$, so that the latter is not affected by the excitation process. Such an inversion of the system into the biexciton state has been demonstrated, both theoretically and experimentally [24]. In the case of a single excitonic transition (two-level system) under pulsed excitation, it is well known that the population inversion follows single-photon Rabi oscillations as a function of the pulse total intensity $\theta = \int \Omega(t) dt$ only, according to the *pulse area theorem*, as $\sin^2(\theta/2)$. In the case of 2P resonant excitation of the biexciton, the oscillations depend also on the pulse shape, duration τ_p and binding energy χ . Only when the pulse becomes very strong, $\theta \gg \chi\tau_p$, one finds the simple relation $\sin^2[\theta/(2\sqrt{2})]$ independent of the pulse characteristics. The pulse should be intense enough in order to fully invert the population into the biexciton state, short (typically of a few picoseconds) in order to minimize the effect of dephasing, and spectrally much narrower than the binding energy in order to minimize the excitation of the intermediate excitonic state [24]. Another promising possibility is the *rapid adiabatic passage* from the ground to the biexciton state via a frequency-sweeping pulse, as proposed in [27]. This has recently been achieved experimentally for the single exciton inversion [28, 29] and has the advantage of being largely unaffected by variation in the dipole coupling or in the optical field, typical of quantum dots. To summarize, coherent control of excitonic states has made significant progress over the last few years [30] and successful manipulation of the biexciton has been reported in several works [24, 25, 31–35]; therefore, we will assume the biexciton in an empty cavity, $|B, 0\rangle$, as the initial state following the pulse. The fact that the probability to excite the biexciton is less than one in an actual experiment does not change qualitatively our results, but merely decreases the efficiency of the mechanism by this probability. The small spurious population of the excitonic intermediate state $|V\rangle$ does not directly affect the results either, because it is disconnected from the cavity dynamics. This is also why the fine structure splitting between $|H\rangle$ and $|V\rangle$ is not important for the physics

⁶ With typical values of $g = 50 \mu\text{eV}$ in the laboratory [22], the other parameters used for the simulation come out as $\chi = 1 \text{ meV}$, $\kappa = 50 \mu\text{eV}$ and $\gamma = 25 \text{ neV}$.

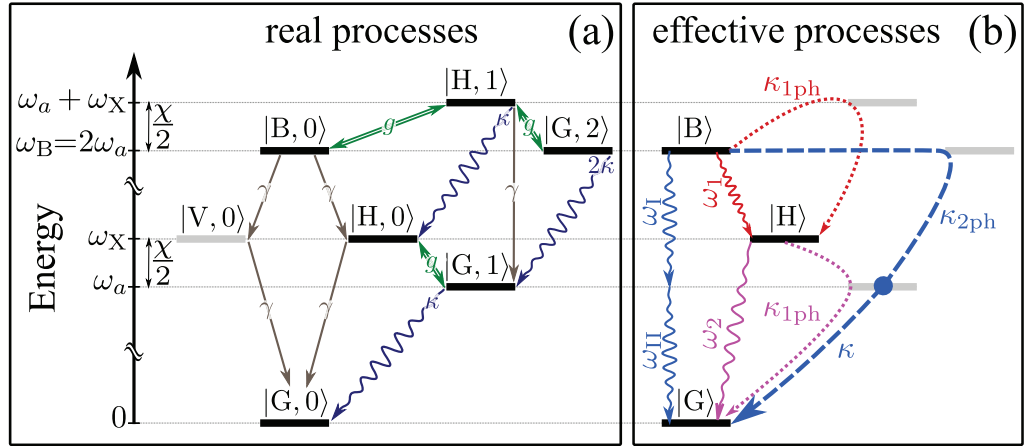


Figure 2. Level scheme of a quantum dot coupled to a cavity mode with linear polarization H at the two-photon resonance. In (a), the microscopic configuration including dot–cavity coupling g , cavity losses κ and excitonic spontaneous decay γ . In (b), the effective processes taking place in the de-excitation of the biexciton through the cavity mode: on the one hand, the emission of two real and distinguishable photons ω_1 and ω_2 (in dotted red and pink), and on the other hand, the simultaneous emission of one 2P state at ω_a (in dashed blue), labeled $\omega_{I,II}$. These three events give rise to the three peaks composing the spectra in figure 1 (with the same color code).

described: while it should be taken into account in the excitation process to ensure the spectral matching with the 2P excitation field (V-polarized), it does not enter the equations that describe the de-excitation process. This recourse to one polarization path only is an additional advantage of our scheme as compared to others that rely on the biexciton decay through *both* of the excitonic paths, such as in the generation of entangled photon pairs [35, 36].

With the previous considerations, the Hamiltonian in the basis of linearly polarized states reads

$$H = \omega_a a^\dagger a + \omega_X(|H\rangle\langle H| + |V\rangle\langle V|) + (2\omega_X - \chi)|B\rangle\langle B| + g[a^\dagger(|G\rangle\langle H| + |H\rangle\langle B|) + \text{h.c.}], \quad (2)$$

where it now appears explicitly that the cavity couples only to its corresponding linear polarization (H). Dissipation affects the bare states, i.e. in the spin-up/spin-down basis, yielding a master equation:

$$\partial_t \rho = i[\rho, H] + \frac{\kappa}{2} \mathcal{L}_a(\rho) + \frac{\gamma}{2} \sum_{i=\uparrow, \downarrow} [\mathcal{L}_{|G\rangle\langle i|} + \mathcal{L}_{|i\rangle\langle B|}](\rho), \quad (3)$$

where $\mathcal{L}_c(\rho) = 2c\rho c^\dagger - c^\dagger c\rho - \rho c^\dagger c$, with κ the cavity losses and γ the exciton relaxation rates. In this study, we assume that $\gamma \ll \kappa$, which is the typical experimental situation. Figure 2 shows the self-consistently truncated configuration of levels involved in the biexciton de-excitation. The coherent coupling (g) is represented by bidirectional green arrows, spontaneous decay (γ) by straight grey arrows and cavity decay (κ) by curly blue arrows, each of them linking in a reversible (g) or irreversible (γ, κ) way the different levels.

A *one-photon resonance* (1PR) is realized when the cavity is set at resonance with one of the excitonic transitions: $|B, 0\rangle \rightarrow |H, 0\rangle$ with frequency $\omega_1 \approx \omega_B - \omega_X$ or $|H, 0\rangle \rightarrow |G, 0\rangle$ with

frequency $\omega_2 \approx \omega_X$. The resonant single-photon emission is then enhanced into the cavity mode according to the conventional scenario [37], with a Purcell decay rate:

$$\gamma_P = 4g^2/\kappa. \quad (4)$$

A *two-photon resonance* (2PR) is realized when the transition $|B, 0\rangle \rightarrow |G, 0\rangle$ matches energetically the emission of two cavity photons [17]:

$$\omega_a \approx \omega_X - \chi/2 \quad \text{with } \chi \gg g, \kappa, \gamma. \quad (5)$$

This process also benefits from Purcell enhancement. In fact, if the decay rates κ and γ are small enough, 2P Rabi oscillations between states $|B, 0\rangle$ and $|G, 2\rangle$ are realized, with a characteristic frequency $g_{2P} \approx 4g^2/(\sqrt{2}\chi)$ [17]. Note that in equation (5), we have neglected the small Stark shifts $\approx g_{2P}$, which should be taken into account to achieve maximum Rabi amplitude. In this paper, to remain within experimentally achievable configurations, we consider systems whose figures of merit are such that the system is in strong coupling at the 1PR, $4g \gtrsim \kappa$. However, the coupling needs not be so large that the system is in strong coupling also at the 2PR. That is, we remain within the 2P weakly coupled regime, $4g_{2P} \ll \kappa$, where 2P oscillations do not actually take place. In these conditions, at the 2PR, the one-photon Rabi oscillations (e.g. $|B, 0\rangle \leftrightarrow |H, 1\rangle$) still take place at the frequency g but, as they are largely detuned, the coupling strength effectively reduces to $g_{1P} \approx g/\sqrt{1 + [\chi/(\gamma + \kappa)]^2} \approx g\kappa/\chi$ [38].

3. Demonstration of the 2P emission at the 2P resonance

To characterize and analyze the main output of the system, shown in figure 1, we study the time-resolved power spectrum $S(t, \omega) \propto \Re \int_0^t dT \int_0^{t-T} d\tau e^{i\omega\tau} \langle a^\dagger(T)a(T+\tau) \rangle$ [39] that we compute as [40]

$$S(t, \omega) = \frac{1}{\pi} \sum_{\alpha \in \{1, 2, I, II, \dots\}} \left(\tilde{L}_\alpha(t, \omega) \frac{\frac{\gamma_\alpha}{2}}{(\frac{\gamma_\alpha}{2})^2 + (\omega - \omega_\alpha)^2} - \tilde{K}_\alpha(t, \omega) \frac{\omega - \omega_\alpha}{(\frac{\gamma_\alpha}{2})^2 + (\omega - \omega_\alpha)^2} \right), \quad (6)$$

where we emphasized in the sum four dominant processes labeled 1, 2, I and II (the results below include all processes). Each α corresponds to a transition in the system, characterized by its frequency (ω_α) and broadening (γ_α), which allow us to identify its microscopic origin, as discussed below. The quantities \tilde{L}_α and \tilde{K}_α are real-valued functions of time and frequency, which correspond, respectively, to the time-integrated signal and its interference with other transitions, up to time t . They tend at infinite time to frequency-independent quantities that we label without tilde, L_α and K_α , corresponding to their full time-integrated values. Therefore, L_α quantifies the total intensity emitted through a given transition α . As such, this is one of the principal quantities of interest in this paper, which is experimentally accessed by conventional photoluminescence measurements. The time-dependent spectra of emission, on the other hand, can be obtained with a streak camera [41].

The system decays via the cavity mode (through the annihilation of a photon a) or via spontaneous emission into the leaky modes (related to the four excitonic lowering operators). With the biexciton state in an empty cavity, $|B, 0\rangle$, as the initial condition, we identify three main de-excitation mechanisms of the system. We now describe them in turn.

1. The first decay route is a cascade of two spontaneous emissions, from $|B\rangle$ to $|H\rangle$ (or $|V\rangle$) in a first time, and then from $|H\rangle$ (or $|V\rangle$) to $|G\rangle$ in a second time, as shown by straight gray

lines in figure 2(a). This decay into leaky modes is at the excitonic energies, ω_1 , ω_2 , and is a direct process with a straightforward microscopic origin as a transition between two states. Each process happens at the rate γ , so that, as far as the biexciton is concerned, its total rate of de-excitation through this channel is 2γ . The effect of this channel is to reduce the efficiency of de-excitation through the cavity mode, which is the one of interest. This can be kept small by choosing a system with a small γ .

2. The second decay route is another cascade of one-photon emissions, but now through the cavity mode, namely from $|B\rangle$ to $|G\rangle$ passing by $|H\rangle$. It is shown by dotted lines in figure 2(b). It effectively amounts to two consecutive photons into the cavity mode at the excitonic energies ω_1 and ω_2 , also shown by curly lines with the same color code in figure 2(b), but the microscopic origin is now more complex, as it involves virtual intermediate states. The first photon, 1, is emitted through the process $|B, 0\rangle \xrightarrow{|H, 1\rangle} |H, 0\rangle$, via the off-resonant ('virtual') state $|H, 1\rangle$ and the second, 2, similarly through the process $|H, 0\rangle \xrightarrow{|G, 1\rangle} |G, 0\rangle$. Due to the dispersive coupling, the initial state in each of these processes (which has no photon) acquires a small component, $C_{1P} = 2g/\chi$, from the corresponding virtual state (which has one photon). It is through this component that it can effectively emit a cavity photon, at rate κ . The effective total decay rate can be understood as the probability to transit to the virtual state times the photon decay rate: $\kappa_{1P} = C_{1P}^2 \kappa$. This derivation leads to the same result as directly computing the Purcell decay rate in the dispersive regime, $\kappa_{1P} = 4g_{1P}^2/\kappa$. We estimate the positions and broadenings of the two resulting spectral peaks ($\alpha = 1, 2$ in equation (6)), by applying the quantum regression theorem within an effective Hilbert space [40] excluding V-polarized and 2P states (none of them being an initial or a final state of the aforementioned processes). The minimal regression matrix to reproduce the main spectral features, including the two transitions under discussion, is 4×4 . With this prescription, $\omega_1 \approx -\chi - 2g^2/\chi$, $\omega_2 \approx 2g^2/\chi$ and $\gamma_1 \approx 3\gamma$, $\gamma_2 \approx \gamma$. The broadenings of the transitions correspond, as expected on physical grounds, to the sum of the decay rates that affect the initial and the final state, without any influence of the virtual ones.
3. Finally, the central event in our proposal is formed by the third channel of de-excitation of the biexciton, namely the emission into the cavity mode of two simultaneous and indistinguishable photons with a frequency very close to that of the cavity $\omega_1 \approx \omega_{II} \approx \omega_a$. This process is sketched by the single dashed blue line in figure 2(b), with an intermediate step marked by a point at $|G, 1\rangle$. Effectively, this amounts to the generation of a 2P state, represented by the two curly transitions $\omega_{I,II}$ in figure 2(b). The two indices I and II strictly correspond to transitions that arise in the spectral decomposition (6), namely $|B, 0\rangle \xrightarrow{|G, 2\rangle} |G, 1\rangle$ for the first sequence of events, I, and the closing of the path, $|G, 1\rangle \rightarrow |G, 0\rangle$, for the second transition, II. Although we have used I and II in figure 2 to label the two photons for the sake of illustration, these two photons are indistinguishable and cannot be interpreted as real events taken in isolation in association with the above sequences of transitions. Indeed, each event gives rise to an unphysical spectrum (assuming negative values) and only when both processes are taken together, they interfere to sum to a physical spectrum which can be interpreted as a probability of (2P) detection. This decomposition of the 2P (central) peak is shown in figure 1 in the time-dependent spectra, with the process I shown by a dotted line and II by a dashed line. They sum to the physical (observable) peak, in solid line. Both peaks grow together in time and develop an asymmetry, one being completely positive, I, the other completely negative, II. None, not even the fully positive peak, can be observed

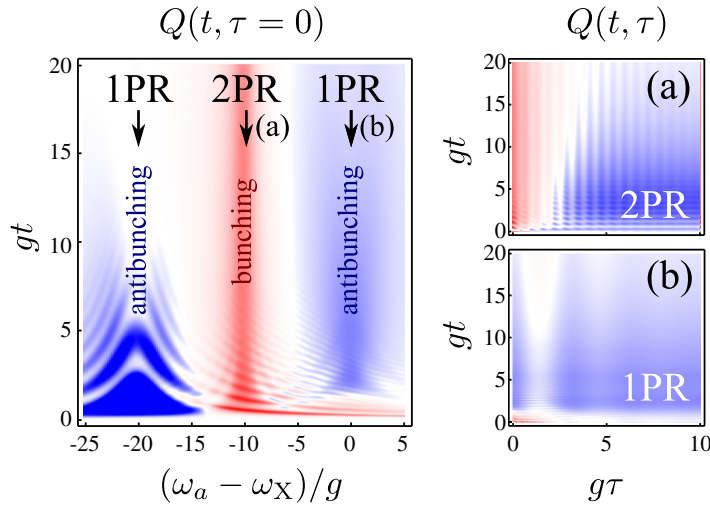


Figure 3. Mandel parameter $Q(t, \tau = 0)$ as a function of the cavity frequency ω_a , for a set of typical parameters ($\chi = 20g, \kappa = g$ and $\gamma = 5 \times 10^{-2}g$). $Q(t, \tau)$ is shown on the right panels at the two relevant resonances: (a) 2P and (b) one-photon. There is a change in the statistics from antibunching <0 (1PR), colored in blue, to bunching >0 (2PR), colored in red.

in isolation. In contrast, the single-photon peaks on both sides (red and pink) are formed by single, isolated transitions, showing their real (as opposed to virtual) nature. The Purcell rate of the 2P emission is again related to the small component of $|G, 2\rangle$ that the initial state $|B, 0\rangle$ grows due to the weak 2P coupling, $C_{2P} = 2\sqrt{2}g^2/(\chi\kappa)$. Given that the rate of photon emission of the state $|G, 2\rangle$ is 2κ , in this case we have $\kappa_{2P} = C_{2P}^2 2\kappa$, equivalent to $\kappa_{2P} = 4g_{2P}^2/(2\kappa)$. Following our analytical approach, we find $\omega_I \approx -\chi/2 + 2g^2/\chi$ with broadening $\gamma_I \approx \kappa + 2\gamma$ (this is the sum of the decay that the initial and final states, $|B, 0\rangle$ and $|G, 1\rangle$, suffer). The other transition, II, stems from the direct process $|G, 1\rangle \rightarrow |G, 0\rangle$. This transition appears at $\omega_{II} \approx -\chi/2 - 2g^2/\chi$ with broadening $\gamma_{II} \approx \kappa$.

A compelling proof of the 2P character of the central peak is given by the time-dependent spectrum (figure 1). Whereas the single-photon events grow in succession—first the L_1 peak that populates the state $|H\rangle$, which subsequently decays to $|G\rangle$, forming the L_2 peak—the 2P peak arises from the joint and simultaneous contribution of the I and II processes. In fact, one can show that at the 2PR, $L_I + L_{II} \approx 2\langle a^{\dagger 2} a^2 \rangle$, linking directly the intensity of the peak with the 2P emission probability. This can be brought to the experimental test by resolving the photon statistics in time, $g^{(2)}(t, \tau) = \langle a^\dagger(t) a^\dagger(t+\tau) a(t+\tau) a(t) \rangle / [n_a(t) n_a(t+\tau)]$, where $n_a = \langle a^\dagger a \rangle$ is the mean cavity photon number. We use the Mandel Q -parameter to illustrate this, $Q(t, \tau) = n_a(t)(g^{(2)}(t, \tau) - 1)$, since it changes sign with the nature of the correlations (negative for anticorrelations). This is shown in figure 3, with a strong and sharp bunching of the emission when the cavity hits the 2P resonance (meaning that photons come together, and in our case, in pairs), while it is antibunched in other cases (photons coming separately). What is remarkable about the 2P emission is that it is consistently bunched at all times: while the system can emit at any time, when it does, it emits the two photons together. In contrast, the 1PR emission is mostly antibunched, as expected, but it also has the possibility to be bunched by fortuitous joint emission of two photons. This is the case when $\omega_a = \omega_2$, the cavity is then in

resonance with the lower transition, which can start only as a successor of the upper transition resulting in a high probability for two-photon detection, but only at very early times, since one photon is a precursor of the other one in a cascade of two otherwise distinguishable events. The proof is complete with the autocorrelation time τ , shown in panels (a) and (b), further demonstrating that in the 2PR emission, the two photons arrive at zero time delay (the emission being less likely again at nonzero delay). Cross-correlation measurements between the three filtered peaks would also show strong features, namely anticorrelations at all delays between all the peaks, with the exception of the positive cross-correlation between 1 and 2 (in this order and with some delay) and positive autocorrelation of the central peak (at zero delay).

4. Efficiency of the 2P emission

Now that we have demonstrated from various points of view the 2P character of the central peak, we aim to maximize it as compared to all other de-excitation channels.

Although we present and plot numerical results of the full master equation (3) throughout the paper, we also provide analytical expressions for the magnitudes of interest. In order to compute intensities of emission, L_α , we need to obtain the full density matrix. As in the case of applying the quantum regression theorem, we can exclude in the derivation the V polarized states. Note, however, that $|G, 2\rangle$ plays a central role in the one-time dynamics and must be included in the estimation of the density matrix elements. There are three key parameters to enhance the 2P emission: κ , γ and χ . The case $\gamma = 0$ is the ideal configuration, where all the emission goes through the cavity:

$$I_a = \int_0^\infty n_a(t) dt = 2/\kappa, \quad (7)$$

which, in the limit $\chi \rightarrow \infty$, is redistributed between the two possible decay paths as

$$L_I + L_2 \approx \frac{\kappa_{1P}}{\kappa_{1P} + \kappa_{2P}} I_a \approx \frac{2}{\gamma_P + \kappa}, \quad (8)$$

$$L_I + L_{II} \approx \frac{\kappa_{2P}}{\kappa_{1P} + \kappa_{2P}} I_a \approx \frac{2\gamma_P/\kappa}{\gamma_P + \kappa}. \quad (9)$$

This is shown in figure 4(a), where we see that the 2P emission dominates over the 1P when $\kappa < 2g$ (shaded in yellow in figure 4(a)), since in this case $\kappa_{2P} > \kappa_{1P}$. For cavities with a high enough quality factor (small κ), the 2P emission is over four orders of magnitude higher than the 1P, showing that the device is extremely efficient for good technological systems [42].

When γ is nonzero—the situation of experimental interest—but is still the smallest parameter ($\gamma \ll \kappa$, $g \ll \chi$), the channel of decay that it opens leads to

$$I_a = \int_0^\infty n_a(t) dt = \frac{\gamma_P(\gamma_P + \kappa)}{\gamma \chi^2}, \quad (10)$$

which is now redistributed between the two cavity decay paths as an increasing function of χ^{-2} :

$$L_I + L_2 \approx \frac{\kappa_{1P}}{\kappa_{1P} + \kappa_{2P} + 2\gamma} I_a \approx \frac{\gamma_P \kappa}{\gamma \chi^2}, \quad (11)$$

$$L_I + L_{II} \approx \frac{\kappa_{2P}}{\kappa_{1P} + \kappa_{2P} + 2\gamma} I_a \approx \frac{\gamma_P^2}{\gamma \chi^2}. \quad (12)$$

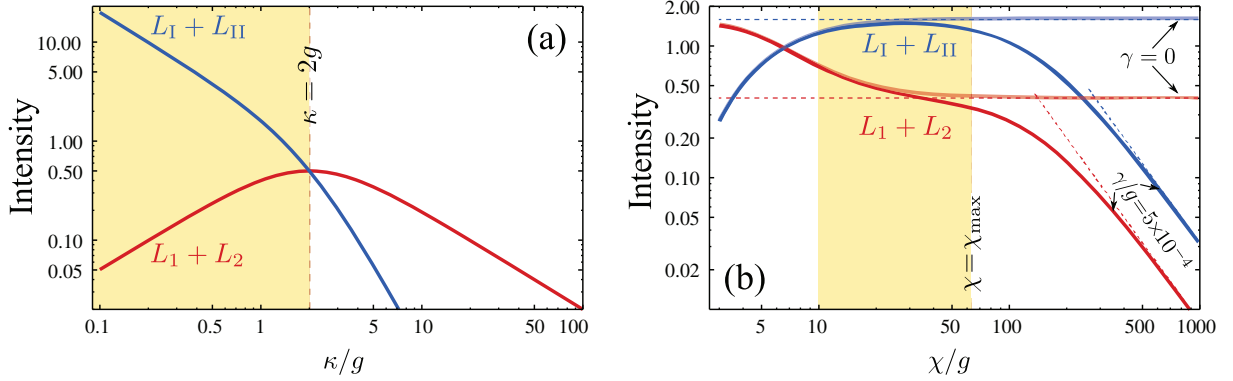


Figure 4. (a) Intensity $L_I + L_{II}$ of emission in the 2P channel (blue) and $L_1 + L_2$ in the two 1P channels (red) as a function of κ , for $\chi \rightarrow \infty$ in the most efficient case $\gamma = 0$. The shaded yellow area $\kappa < 2g$ shows the region where the 2P emission dominates. (b) Same as before for $\kappa = g$ as a function of χ , that must be large enough so that 1P are suppressed and small enough to maintain a high cavity emission efficiency in the realistic case of nonzero γ .

This nonzero γ case is shown in figure 4(b), where the most efficient situation can be recovered in a region of χ bounded above by

$$\chi_{\max} = \min\left(2g\sqrt{\kappa/(2\gamma)}, 4g^2/\sqrt{2\kappa\gamma}\right), \quad (13)$$

which follows from $2\gamma = \min(\kappa_{1P}, \kappa_{2P})$. Above χ_{\max} , the 2P emission still dominates over 1P emission but efficiency is spoiled, according to equations (11), which are shown by dashed tilted lines.

5. Conclusions and outlook

In conclusion, we have presented a scheme where the biexciton is in 2P resonance with a microcavity mode, as an efficient 2P source, both in terms of the purity of the 2P state and of its emission efficiency. The timescale for 2P emission, which limits the repetition rate, is of the order of κ_{2P}^{-1} and the linewidth of the 2P peak $\approx \kappa$ is determined by the cavity quality factor. The quantum character of the 2P emission is demonstrated theoretically by a detailed analysis of all the processes involved in the biexciton de-excitation, which also allows us to find analytically the optimum conditions for its realization. We have shown that the 2Ps are emitted simultaneously with no delay in the autocorrelation time. Experimentally, the ultimate proof of indistinguishability can be obtained by directing the central peak to a beam splitter, which half of the time will separate the photon pair into two ports that can then be fed in a Hong–Ou–Mandel interferometer.

Acknowledgments

We thank F Troiani, D Sanvitto, A Laucht and J J Finley for discussions. We acknowledge support from the Emmy Noether project HA 5593/1-1 (DFG), the Alexander von Humboldt

Foundation, the Marie Curie IEF ‘SQOD’, the Spanish MICINN (MAT2008-01555 and CSD2006-00019-QOIT), CAM (S-2009/ESP-1503) and the FPU program (AP2008-00101) from the Spanish Ministry of Education.

References

- [1] Nagata T, Okamoto R, O’Brien J L, Sasaki K and Takeuchi S 2007 Beating the standard quantum limit with four-entangled photons *Science* **316** 726
- [2] Simon C, de Riedmatten H, Afzelius M, Sangouard N, Zbinden H and Gisin N 2007 Quantum repeaters with photon pair sources and multimode memories *Phys. Rev. Lett.* **98** 190503
- [3] Cirac J I, Zoller P, Kimble H J and Mabuchi H 1997 Quantum state transfer and entanglement distribution among distant nodes in a quantum network *Phys. Rev. Lett.* **78** 3221
- [4] Duan L-M, Lukin M D, Cirac J I and Zoller P 2001 Long-distance quantum communication with atomic ensembles and linear optics *Nature* **414** 413
- [5] Santori C, Fattal D, Vukovick J, Solomon G S and Yamamoto Y 2002 Indistinguishable photons from a single-photon device *Nature* **419** 594
- [6] Kok P, Munro W J, Nemoto K, Ralph T C, Dowling J P and Milburn G J 2007 Linear optical quantum computing with photonic qubits *Rev. Mod. Phys.* **79** 135
- [7] Lanyon B P, Weinhold T J, Langford N K, O’Brien J L, Resch K J, Gilchrist A and White A G 2008 Manipulating biphotonic qutrits *Phys. Rev. Lett.* **100** 060504
- [8] Cancellieri E, Troiani F and Goldoni G 2009 Optimal generation of indistinguishable photons from non-identical artificial molecules *Opt. Express* **17** 17156
- [9] Sangouard N, Simon C, de Riedmatten H and Gisin N 2011 Quantum repeaters based on atomic ensembles and linear optics *Rev. Mod. Phys.* **83** 33
- [10] Aspect A, Grangier P and Roger G 1982 Experimental realization of Einstein–Podolsky–Rosen–Bohm Gedankenexperiment: a new violation of Bell’s inequalities *Phys. Rev. Lett.* **49** 91
- [11] Collins D, Gisin N, Linden N, Massar S and Popescu S 2002 Bell inequalities for arbitrarily high-dimensional systems *Phys. Rev. Lett.* **88** 040404
- [12] Thompson J K, Simon J, Loh H and Vuletić V 2006 A high-brightness source of narrowband, identical-photon pairs *Science* **313** 74
- [13] Balić V, Braje D A, Kolchin P, Yin G Y and Harris S E 2005 Generation of paired photons with controllable waveforms *Phys. Rev. Lett.* **94** 183601
- [14] Du S, Kolchin P, Belthangady C, Yin G Y and Harris S E 2008 Subnatural linewidth biphotons with controllable temporal length *Phys. Rev. Lett.* **100** 183603
- [15] Scholz M, Koch L and Benson O 2009 Statistics of narrow-band single photons for quantum memories generated by ultrabright cavity-enhanced parametric down-conversion *Phys. Rev. Lett.* **102** 063603
- [16] Akiba K, Kashiwagi K, Arikawa M and Kozuma M 2009 Storage and retrieval of nonclassical photon pairs and conditional single photons generated by the parametric down-conversion process *New J. Phys.* **11** 013049
- [17] del Valle E, Zippilli S, Laussy F P, Gonzalez-Tudela A, Morigi G and Tejedor C 2010 Two-photon lasing by a single quantum dot in a high- Q microcavity *Phys. Rev. B* **81** 035302
- [18] Akopian N, Lindner N H, Poem E, Berlatzky Y, Avron J, Gershoni D, Gerardot B D and Petroff P M 2006 Entangled photon pairs from semiconductor quantum dots *Phys. Rev. Lett.* **96** 130501
- [19] Hafenbrak R, Ulrich S M, Michler P, Wang L, Rastelli A and Schmidt O G 2007 Triggered polarization-entangled photon pairs from a single quantum dot up to 30 K *New J. Phys.* **9** 315
- [20] Ates S, Ulrich S M, Ulhaq A, Reitzenstein S, Löffler A, Höfling S, Forchel A and Michler P 2009 Non-resonant dot–cavity coupling and its potential for resonant single-quantum-dot spectroscopy *Nat. Photonics* **3** 724

- [21] Ates S, Ulrich S M, Reitzenstein S, Löffler A, Forchel A and Michler P 2009 Post-selected indistinguishable photons from the resonance fluorescence of a single quantum dot in a microcavity *Phys. Rev. Lett.* **103** 167402
- [22] Ota Y, Iwamoto S, Kumagai N and Arakawa Y 2011 Spontaneous two photon emission from a single quantum dot arXiv:1107.0372
- [23] Machnikowski P 2008 Theory of two-photon processes in quantum dots: coherent evolution and phonon-induced dephasing *Phys. Rev. B* **78** 195320
- [24] Stuffer S, Machnikowski P, Ester P, Bichler M, Axt V M, Kuhn T and Zrenner A 2006 Two-photon Rabi oscillations in a single $\text{In}_x\text{Ga}_{1-x}\text{As}/\text{GaAs}$ quantum dot *Phys. Rev. B* **73** 125304
- [25] Chen G, Stievater T H, Batteh E T, Li X, Steel D G, Gammon D, Katzer D S, Park D and Sham L J 2002 Biexciton quantum coherence in a single quantum dot *Phys. Rev. Lett.* **88** 117901
- [26] Boyle S J, Ramsay A J, Fox A M and Skolnick M S 2010 Two-color two-photon Rabi oscillation of biexciton in single InAs/GaAs quantum dot *Physica E* **42** 2485
- [27] Hui H Y and Liu R B 2008 Proposal for geometric generation of a biexciton in a quantum dot using a chirped pulse *Phys. Rev. B* **78** 155315
- [28] Simon C M *et al* 2011 Robust quantum dot exciton generation via adiabatic passage with frequency-swept optical pulses *Phys. Rev. Lett.* **106** 166801
- [29] Wu Y, Piper I M, Ediger M, Brereton P, Schmidgall E R, Eastham P R, Hugues M, Hopkinson M and Phillips R T 2011 Population inversion in a single InGaAs quantum dot using the method of adiabatic rapid passage *Phys. Rev. Lett.* **106** 067401
- [30] Ramsay A J 2010 A review of the coherent optical control of the exciton and spin states of semiconductor quantum dots *Semicond. Sci. Technol.* **25** 103001
- [31] Flissikowski T, Betke A, Akimov I A and Henneberger F 2004 Two-photon coherent control of a single quantum dot *Phys. Rev. Lett.* **92** 227401
- [32] Akimov I A, Andrews J T and Henneberger F 2006 Stimulated emission from the biexciton in a single self-assembled II–VI quantum dot *Phys. Rev. Lett.* **96** 067401
- [33] Boyle S J, Ramsay A J, Fox A M and Skolnick M S 2009 Beating of exciton-dressed states in a single semiconductor $\text{InGaAs}/\text{GaAs}$ quantum dot *Phys. Rev. Lett.* **102** 207401
- [34] Miyazawa T, Kodera T, Nakaoka T, Watanabe K, Kumagai N, Yokoyama N and Arakawa Y 2010 Two-photon control of biexciton population in telecommunication-band quantum dot *Appl. Phys. Express* **3** 064401
- [35] Dousse A, Suffczyński J, Beveratos A, Krebs O, Lemaître A, Sagnes I, Bloch J, Voisin P and Senellart P 2010 Ultrabright source of entangled photon pairs *Nature* **466** 217
- [36] Stevenson R M, Young R J, Atkinson P, Cooper K, Ritchie D A and Shields A J 2006 A semiconductor source of triggered entangled photon pairs *Nature* **439** 179
- [37] Gérard J-M, Sermage B, Gayral B, Legrand B, Costard E and Thierry-Mieg V 1998 Enhanced spontaneous emission by quantum boxes in a monolithic optical microcavity *Phys. Rev. Lett.* **81** 1110
- [38] Laussy F P, del Valle E and Tejedor C 2009 Luminescence spectra of quantum dots in microcavities. I. Bosons *Phys. Rev. B* **79** 235325
- [39] Eberly J H and Wódkiewicz K 1977 The time-dependent physical spectrum of light *J. Opt. Soc. Am.* **67** 1252
- [40] del Valle E, Laussy F P and Tejedor C 2009 Luminescence spectra of quantum dots in microcavities. II. Fermions *Phys. Rev. B* **79** 235326
- [41] Wiersig J *et al* 2009 Direct observation of correlations between individual photon emission events of a microcavity laser *Nature* **460** 245
- [42] Nomura M, Ota Y, Kumagai N, Iwamoto S and Arakawa Y 2008 Large vacuum Rabi splitting in single self-assembled quantum dot–nanocavity system *Appl. Phys. Express* **1** 072102